Universal Existence of Localized Single-Photon Emitters in the Perovskite Film of All-Inorganic CsPbBr₃ Microcrystals

Shengnan Feng, Qilin Qin, Xiaopeng Han, Chunfeng Zhang, Xiaoyong Wang,* Tao Yu,* and Min Xiao*

All-inorganic halide perovskites have drawn a lot of research attention very recently owing to their potential solution to the instability issue currently faced by the organic–inorganic counterparts. Meanwhile, the halide perovskites in a solid film are manifested as microscale morphologies whose functionalities are unavoidably affected by the interior or exterior presence of various nanoscale entities. Here all-inorganic solid films are fabricated with varying densities of single CsPbBr₃ microcrystals, showing that very sharp photoluminescence peaks can be universally observed at 4 K with the linewidths being as narrow as hundreds of μeV. The single-photon emission nature is confirmed for such a photoluminescence peak, whose intensity is completely quenched above ≈30 K to suggest its possible origin from a low potential-energy region of the single microcrystal. The discovery of such a novel emitting species in halide perovskites, with the enriched structure–property relationship, will surely impart significant influences on the advancement of relevant optoelectronic devices and quantum-light sources.

1. Introduction

Semiconductor halide perovskites are featured with superior optoelectronic properties such as large absorption coefficient, slow carrier recombination, and long charge transport, which can be easily achieved from a cheap solution-processing route and are beneficial for the efficient operations of various functional devices.[1–5] Especially in the photovoltaic area, the power conversion efficiently of solar cells based on organic–inorganic halide perovskites have been tremendously elevated from the initial ≈3.8% to the current ≈25.5% after just one decade of intensive research.[1,6–10] However, the further advancement of

S. Feng, Q. Qin, X. Han, C. Zhang, X. Wang, T. Yu, M. Xiao
School of Physics
National Laboratory of Solid State Microstructures
Collaborative Innovation Center of Advanced Microstructures
Nanjing University
Nanjing 210093, China
E-mail: wxiaoyong@nju.edu.cn; yutao@nju.edu.cn
M. Xiao
Department of Physics
University of Arkansas
Fayetteville, AR 72701, USA
E-mail: mxiao@uark.edu

these solar-cell devices toward the ultimate goal of commercialization is hindered by the instability issue of organic–inorganic halide perovskites due to the existence of organic $CH_3NH_3^+$ (MA⁺) or $(NH_2)_2^+$ (FA⁺) cations.[11–14] As such, a lot of research efforts are now being devoted to the replacements of MA⁺ and FA⁺ by Cs⁺, with the resultant all-inorganic halide perovskites such as CsPbBr₃ being highly robust against the harsh thermal and humid environments.[15–21] So far, the power conversion efficiency of CsPbBr₃-based solar cells has already surmounted 10% and, as in the organic–inorganic case, its further increment is critically dependent on a comprehensive understanding of the structure–property relationship inherent in the all-inorganic films.[22–27]

As has been well documented in the literature,[28,29] the solid film of halide perovskites is composed of different-sized microcrystals that are separated from each other by the grain boundary. The grain boundary contains a large amount of recombination centers and defect sites to cause complex dynamic behaviors of the charge carriers, thus greatly influencing the device operations of a halide perovskite film.[28–30] It has been further revealed that space charges can pile up at the grain boundary to trigger the phase-segregation effect commonly observed in the mixed-halide perovskites.[31,32] The microcrystal itself is also associated with very rich optical phenomena in a halide perovskite film, one of which is the photoluminescence (PL) blinking effect without single-photon emission.[33] This anomalous optical phenomenon can be attributed to the migration of charge carriers among nearby microcrystals, the accumulation of charge carriers at the microcrystal surfaces and boundaries, or the transient appearance of a super trap within the internal of a single microcrystal.[34–37] The above grain-boundary and microcrystal properties obtained from organic–inorganic halide perovskites should be also reflected in the all-inorganic ones, whose detailed optical explorations could provide an alternative view on the complex dynamic processes of charge carriers in these two types of important photovoltaic and light-emitting materials.

Here we have fabricated compact, porous and islanded films of all-inorganic CsPbBr₃ microcrystals with decreasing densities, and performed spatially resolved optical measurements on them at both the room and cryogenic temperatures. At the

room temperature, the compact and porous films are featured with an inhomogeneous distribution of bright and dark emission regions, and the PL blinking effect is observed only from the single $CsPbBr_3$ microcrystals contained in the islanded film. While the above observations are on a par with those already reported for organic–inorganic halide perovskites, we have additionally resolved very sharp PL peaks from all three types of all-inorganic films at the cryogenic temperature of 4 K. PL linewidths of these peaks are as narrow as hundreds of μeV and, due to the reduced background fluorescence, their single-photon emission nature can be easily confirmed from the single $CsPbBr_3$ microcrystals in the islanded film. PL intensity of such a single-photon emitter is completely quenched above ≈30 K, suggesting that it should originate from a low potential-energy region in the single $CsPbBr_3$ microcrystal due to the local variation of its thickness.

2. Results and Discussion

The compact and porous $CsPbBr_3$ films studied here are prepared using a two-step solution deposition method, while a single-step approach is employed to deposit single $CsPbBr_3$ microcrystals in the islanded film (see more details in the Experimental Section). In **Figure 1**a,b, we present the scanning electron microscopy images measured for the compact and porous films, respectively, while the one for the islanded film

is shown in **Figure 2**a. The single $CsPbBr_3$ microcrystals are closely stacked in the compact film, and they are more isolated from each other in the porous and islanded films, with a spatial separation being normally larger than ≈400 nm in the latter case. According to the statistical histograms plotted in Figure S1 in the Supporting Information, the average sizes of the single $CsPbBr_3$ microcrystals in the compact, porous and islanded films are estimated to be ≈322.1, ≈313.0, and ≈133.9 nm, respectively. For the optical measurements performed at the room and cryogenic temperatures, the above three types of $CsPbBr_3$ films are excited at the pulsed laser wavelengths of 405 and 520 nm, respectively (see more details in the Experimental Section).

At the room temperature and under the 405 nm pulsed laser excitation at the power density of ≈14.0 W cm^{-2}, the confocal scanning optical images measured for the compact and porous $CsPbBr_3$ films are demonstrated in Figure 1c,d, respectively. The bright spots observed therein should originate from the optical emission of single $CsPbBr_3$ microcrystals, whose sizes are relatively larger than the ≈300 nm diameter of the excitation laser beam. Meanwhile, the grain boundaries give rise to a lot of dark regions in between the bright spots, and this inhomogeneous distribution of spatial PL intensities is consistent with what was previously reported by de Quilettes et al. in their optical studies of organic–inorganic $MAPbI_3$ films.[28] For one bright spot (blue circle) and one dark region (green square) representatively marked in Figure 1c from the compact film, the corresponding PL spectra are plotted in Figure 1e with the peak
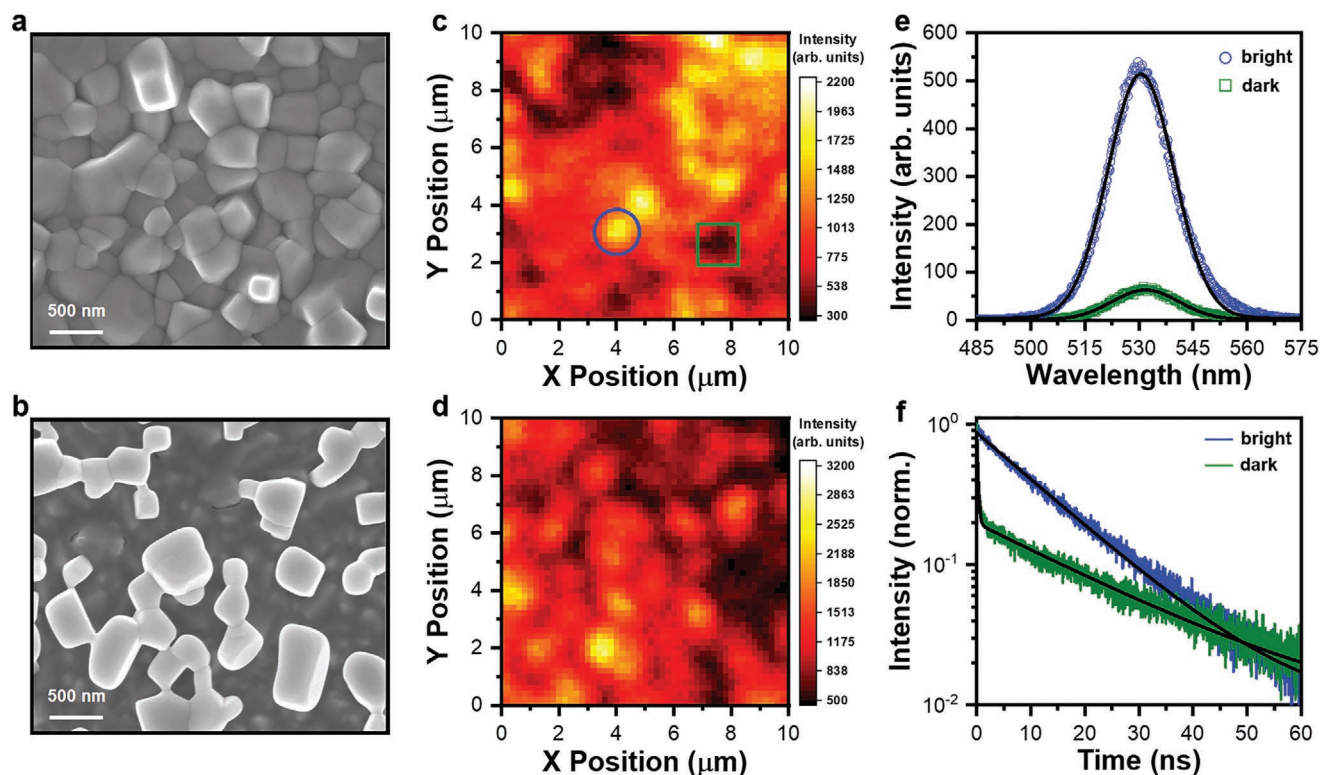

Figure 1. Room-temperature structural and optical characterizations of the compact and porous $CsPbBr_3$ films. a) Scanning electron microscopy image of the compact film. b) Scanning electron microscopy image of the porous film. c) Confocal scanning optical image of the compact film. d) Confocal scanning optical image of the porous film. e) PL spectra measured for the bright spot and dark region marked in (c) by the blue circle and green square, respectively. f) PL decay curves measured for the bright spot and dark region and fitted by the single- and biexponential functions, respectively.
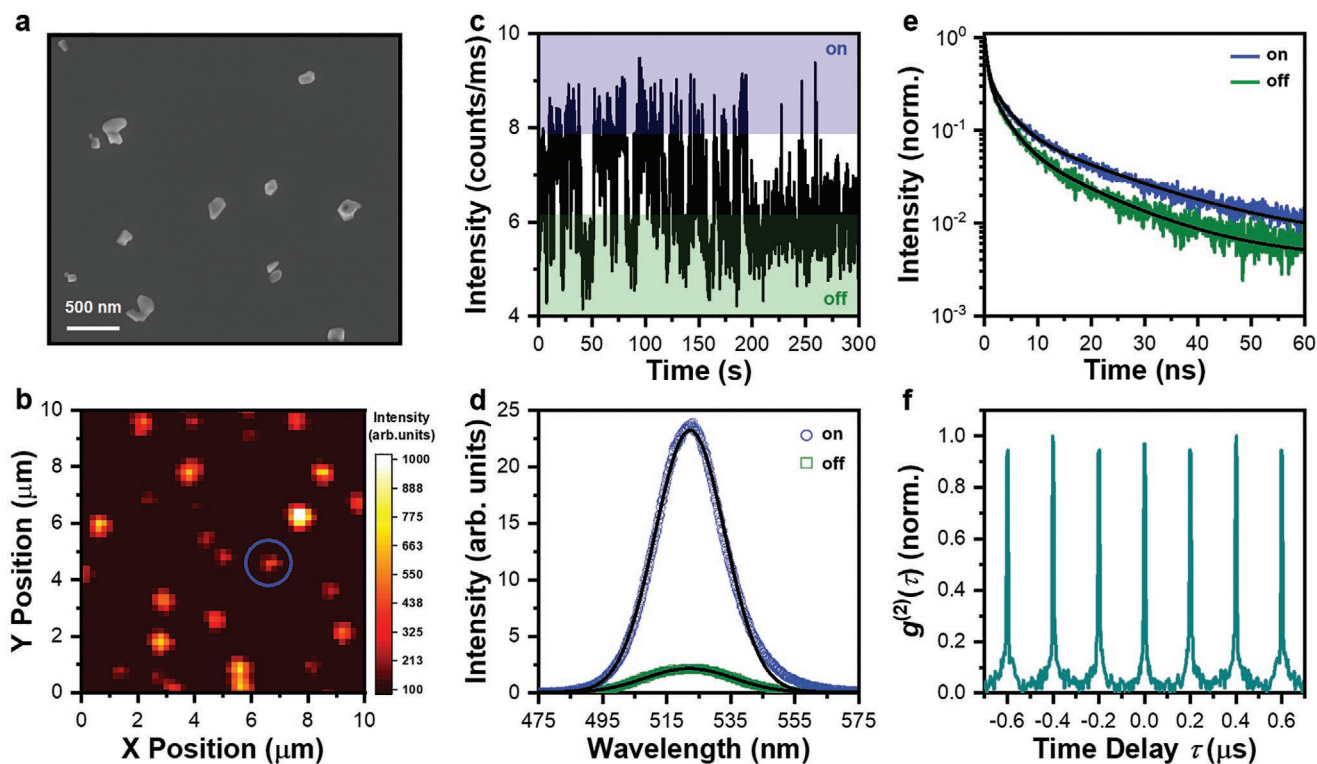
Figure 2. Room-temperature structural and optical characterizations of the islanded CsPbBr$_3$ film. a) Scanning electron microscopy image of the islanded film. b) Confocal scanning optical image of the islanded film. c) PL intensity time trace measured with a binning time of 100 ms for the bright spot marked in (b) by the blue circle. The blinking on and off periods are shaded by the blue and green colors, respectively. d) PL spectra measured for the blinking on and off periods. e) PL decay curves measured for the blinking on and off periods and each fitted by a triexponential function. f) Second-order photon correlation $g^{(2)}(\tau)$ measurement of the blinking on periods.

wavelengths of ≈530.5 and ≈531.7 nm, and the linewidths of ≈21.7 and ≈22.0 nm, respectively. As shown in Figure 1f, the PL decay curve measured for the bright spot is fitted with a single-exponential lifetime of ≈12.92 ns, while that for the dark region can only be fitted well by a biexponential function with the fast and slow lifetimes of ≈0.24 and ≈21.98 ns, respectively.

Based on the significantly reduced PL intensity by almost one order of magnitude, as compared to that of the bright spot, and the appearance of an extremely fast PL lifetime component, it can be deduced that the photoexcited charge carriers in the dark region should be dominantly dissipated by the non-radiative defect sites. We have also performed time-dependent PL intensity measurements on a statistically large number of bright spots in the compact and porous films, without seeing the PL blinking effect (see Figure S2, Supporting Information). This suggests that the migration of charge carriers is either completely absent or very efficient[38] in these two types of CsPbBr$_3$ films, so that the probability for their local accumulation is effectively reduced without causing the PL blinking effect previously observed in the organic–inorganic MAPbBr$_3$ microcrystals.[35]

To further explore the optical properties of single CsPbBr$_3$ microcrystals at the room temperature, we next switch to the islanded film wherein the bright spots can be studied one by one to avoid the possible influence of grain boundaries. As can be seen from Figure 2b under the 405 nm pulsed laser excitation at ≈14.0 W cm^{-2}, the bright spots from single CsPbBr$_3$ microcrystals are well isolated from each other in the confocal scanning optical image. For a representative bright spot marked in Figure 2b by the blue circle, the PL intensity time trace is plotted in Figure 2c where intermittent transitions between the blinking on and off periods can be clearly observed. The PL spectra measured for the on and off periods in Figure 2d are both centered at ≈522.0 nm with the same linewidth of ≈26.6 nm, while their respective lifetimes are averaged at ≈14.0 and ≈9.6 ns from triexponential fittings of the corresponding PL decay curves shown in Figure 2e. As shown in Figure 2f, such a blinking single CsPbBr$_3$ microcrystal is incapable of emitting single photons, with a $g^{(2)}(0)$ value of ≈1.0 being estimated from the second-order photon correlation measurement. The optical properties measured for another bright spot in the islanded film are shown in Figure S3 in the Supporting Information, stressing again the common observation that a blinking microcrystal is lack of the single-photon emission feature, which was similarly observed by Eremchev et al. in their optical studies of single MAPbI$_3$ microcrystals.[33]

So far, the PL blinking effect has been observed in various single-photon emitters, the most typical of which are single organic molecules and colloidal nanocrystals.[39–44] However, it has also been demonstrated occasionally that the PL blinking effect is not necessarily accompanied by the single-photon emission feature, such as in the material systems of germanium-vacancy color centers in microdiamonds,[45] multichromophoric conjugated polymers,[46,47] and single microcrystals of
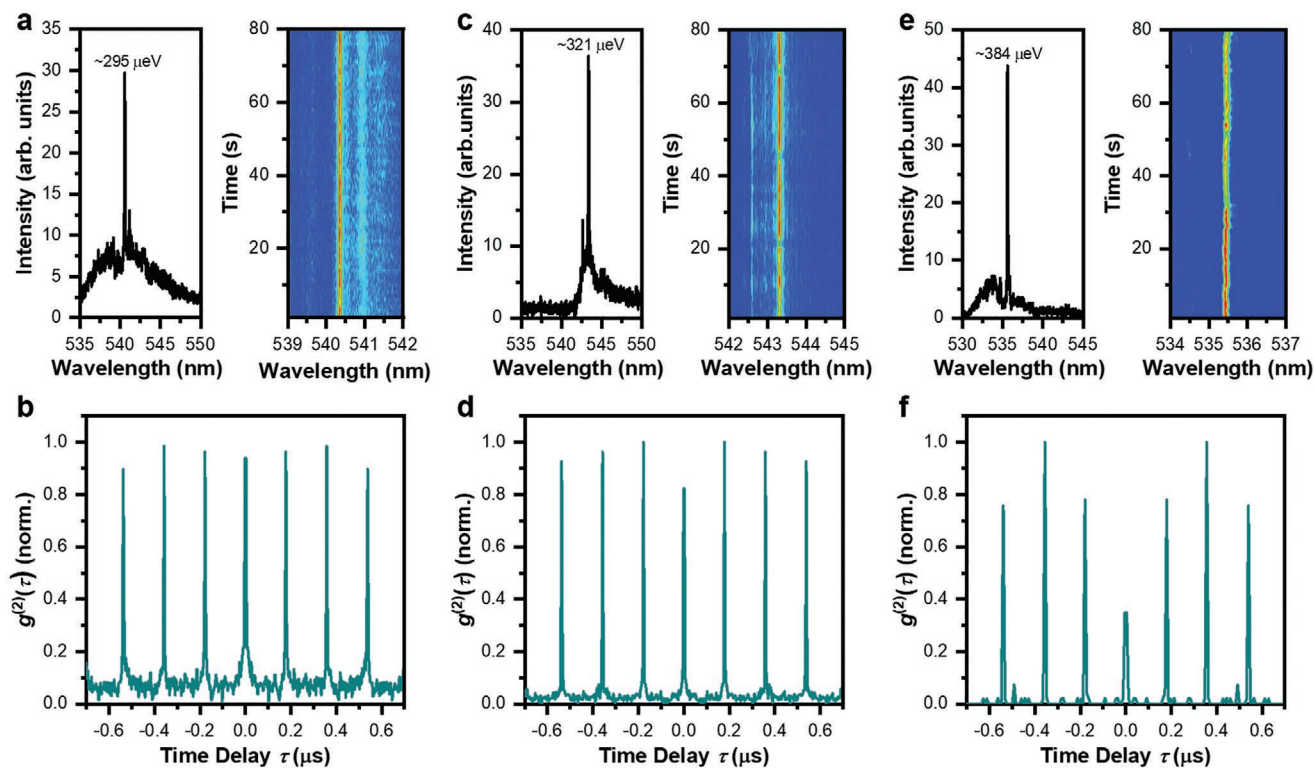
**ADVANCED
SCIENCE NEWS**

www.advancedsciencenews.com

**ADVANCED
MATERIALS**

www.advmat.de

Figure 3. 4 K optical measurements on the three types of CsPbBr$_3$ films. a) PL spectrum (left panel) and time-dependent spectral image (right panel) measured for a bright spot in the compact film. b) Second-order photon correlation measurement of the main sharp PL peak shown in (a) with a linewidth of ≈295 µeV. c) PL spectrum (left panel) and time-dependent spectral image (right panel) measured for a bright spot in the porous film. d) Second-order photon correlation measurement of the main sharp PL peak shown in (c) with a linewidth of ≈321 µeV. e) PL spectrum (left panel) and time-dependent spectral image (right panel) measured for a microcrystal in the islanded film. f) Second-order photon correlation measurement of the main sharp PL peak shown in (e) with a linewidth of ≈384 µeV.

organic–inorganic perovskites.[33] As proposed in the latter case that is more relevant to our current work, the blinking on and off periods observed in single MAPbI$_3$ microcrystals should be caused by the temporal passivation and activation of a super trap related to the migration of ions or impurities.[37] We believe that the above scenario should be also applicable to the single CsPbBr$_3$ microcrystals studied here in the all-inorganic islanded film, wherein the super trap can introduce a nonradiative recombination center for the charge carriers excited in its immediate vicinity to yield the blinking off periods. Meanwhile, the remote charge carriers can still recombine radiatively in the otherwise trap-free regions, thus explaining the same PL peaks and the comparable PL lifetimes measured for the blinking on and off periods in Figure 2d,e, respectively.

The above optical properties measured at the room temperature are quite similar to those already reported for organic–inorganic perovskites, however, very unique emission species are universally discovered at 4 K from all three types of CsPbBr$_3$ films excited at ≈1.4 W cm^{-2} by the pulsed 520 nm laser. As shown in the left panel of **Figure 3**a for a representative bright spot in the compact film, on top a broad background spectrum, a very sharp PL peak emerges with a central wavelength of ≈540.6 nm and a linewidth of ≈295 µeV. Compared to the room-temperature measurement in Figure 1e, the PL peak of a single CsPbBr$_3$ microcrystal in the compact film (also applied to the porous and islanded

films) is shifted to the red side at the cryogenic temperature, which is caused by the unique thermal expansion and exciton-phonon coupling effects of semiconductor perovskites.[48,49] The time-dependent evolution of this PL peak is plotted in the right panel of Figure 3a with an almost stable intensity, and it possesses a $g^{(2)}(0)$ value of ≈0.93 based on the second-order photon correlation measurement shown in Figure 3b. This kind of sharp PL peaks can also be resolved from nearly all the bright spots located on the porous film, one of which is plotted in the left panel of Figure 3c with a central wavelength of ≈543.4 nm and a linewidth of ≈321 µeV. This PL peak suffers occasionally from the PL blinking effect, as can be seen from the time-dependent spectral image plotted in the right panel of Figure 3c, and has a $g^{(2)}(0)$ value of ≈0.82 according to the second-order photon correlation measurement shown in Figure 3d, suggesting that single photons are partially emitted from it albeit with a low purity.

Similar to the compact- and porous-film cases, the sharp PL peaks are also present in all the single CsPbBr$_3$ microcrystals studied in the islanded film. For a representative PL peak shown in the left panel of Figure 3e, the central wavelength is located at ≈535.6 nm with a linewidth of ≈384 µeV, while the PL blinking and spectral diffusion effects can be obviously observed from its time-dependent spectral image plotted in the right panel of Figure 3e. Most impressively, the $g^{(2)}(0)$ value is significantly reduced to ≈0.44 based on the second-order photon

correlation measurement shown in Figure 3f, implying that this PL peak is emanated from a quantum emitter meeting the single-photon emission criterion.[50] In Figure S4 in the Supporting Information, we demonstrate similar optical properties measured for another two single CsPbBr$_3$ microcrystals in the islanded film, whose $g^{(2)}(0)$ values are estimated to be ≈0.39 and ≈0.54, respectively. In our second-order photon correlation measurement, a spectral resolution of ≈1 meV is used to select either the sharp PL peak or the background spectrum emitted from a single CsPbBr$_3$ microcrystal, the latter of which has a $g^{(2)}(0)$ value of ≈1.0 without the single-photon emission feature. The $g^{(2)}(0)$ value should approach zero for a high-purity single-photon emitter,[51] however, the small overlap with the background spectrum (Figure 3e, left panel) makes the sharp PL peak deviate from this perfection. In analogy to this, the sharp PL peaks observed from the compact and porous films should also carry the single-photon emission feature, whose purity is significantly degraded by the background spectra with even larger overlaps (Figure 3a,c, left panels). Besides the main sharp PL peaks discussed above, it can be noticed from the PL spectra shown in Figure 3a,c,e that there exist additional ones on their blue or red sides with much smaller intensities. In Figure S5a,b in the Supporting Information, we provide two more PL spectra measured for the compact and porous films, respectively, showing further that it is quite common to observe several sharp PL peaks from a single bright spot of the CsPbBr$_3$ microcrystal.

As mentioned earlier in the text and shown in Figure S1 in the Supporting Information, the average sizes of single microcrystals in the three types of CsPbBr$_3$ films are significantly larger than the Bohr diameter of ≈7 nm.[52] It is then unlikely for the sharp PL peak to originate from a single microcrystal as a whole, since it does not possess any quantum-confinement effect to yield discrete energy-level structures. As was recently reported for the organic–inorganic FAPbI$_3$ film, the excess amount of FAI relative to that of PbI$_2$ used in the synthesis would facilitate the formation of single-photon emitters from localized nanodomains due to a nonhomogeneous distribution of the organic cations.[53] The above scenario is largely unapplicable to the all-inorganic films studied here with a stoichiometric composition, so we propose instead that multiple low potential-energy regions are naturally formed in the fabrication of a single CsPbBr$_3$ microcrystal as a result of the spatial variation in its thickness. In this case, the sharp PL peaks and the broad background spectrum are contributed by these low potential-energy regions and their surrounding bulk material, respectively, which are reminiscent of those emitted by the single quantum dots (QDs) and the underlying quantum well in an epitaxially grown GaAs sample with an inhomogeneous thickness distribution.[54]
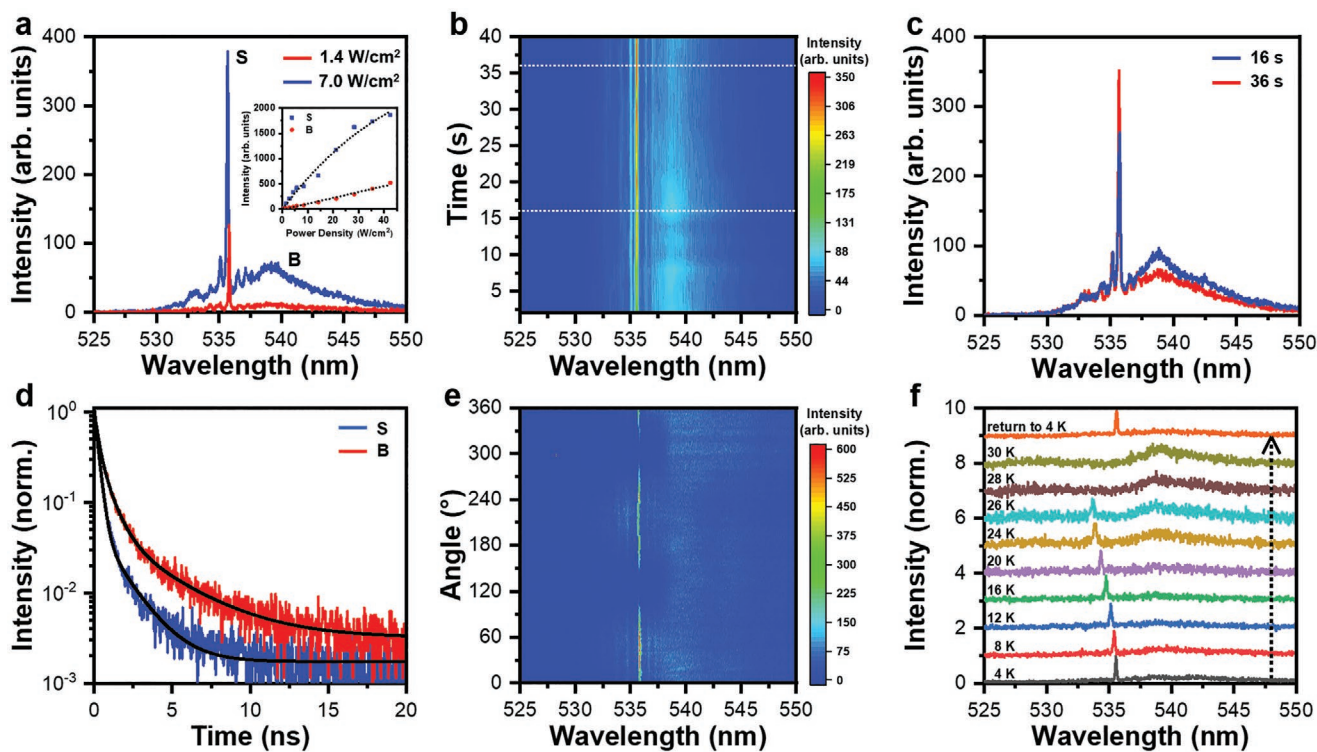

Figure 4. 4 K optical measurements of a single-photon emitter in the islanded CsPbBr$_3$ microcrystal. a) PL spectra measured at the laser power densities of ≈1.4 and ≈7.0 W cm^{-2}, respectively, where a strong sharp PL peak (denoted by S) and a broad background spectrum (denoted by B) can be observed. Inset: PL intensities of the S peak and the B spectrum measured as a function of the laser power density, with the dotted lines being just guides for the eye. b) Time-dependent spectral image measured for this single microcrystal. c) PL spectra extracted from (b) at 16 and 36 s, showing a negative correlation between the intensities of the S peak and the B spectrum. d) PL decay curves measured for the S peak and the B spectrum, and each fitted by a triexponential function. e) Polarization-dependent spectral image measured for this single microcrystal. f) PL spectra measured for this single microcrystal at the increasing temperatures from 4 to 30 K and then at 4 K again. These PL spectra are offset to each other for clarity. In (b)–(f), the single microcrystal is excited at the laser power density of ≈7.0 W cm^{-2}.

In the following, we focus on a single $CsPbBr_3$ microcrystal from the islanded film and plot in **Figure 4**a its 4 K PL spectra measured at the 520 nm pulsed laser power densities of ≈1.4 and ≈7.0 W cm^{-2}, respectively. Each spectrum is comprised of a strong PL peak (denoted by "S"), a broad background spectrum (denoted by "B"), and several weak PL peaks that are more evident at the higher laser power. As shown in the inset of Figure 4a with the increasing laser power, PL intensity of the S peak gets saturated gradually while that of the B spectrum keeps moving up with a linear trend (see Figure S6, Supporting Information, for another example), thus verifying their respective origins from a single QD and the bulk material.[53] The time-dependent spectral image measured for this single $CsPbBr_3$ microcrystal is plotted in Figure 4b, from which two PL spectra are extracted at 16 and 36 s to demonstrate in Figure 4c a slight occurrence of the PL blinking effect. It is interesting to see that PL intensities of the S peak and the B spectrum are negatively correlated, implying that the single QD and the bulk material would compete with each other for the capture of photoexcited charge carriers in a single $CsPbBr_3$ microcrystal.[55]

Besides obvious differences in the central wavelengths and PL linewidths, the S peak and B spectrum are associated with the short and long average lifetimes of ≈0.56 and ≈1.28 ns, respectively, which are estimated from the triexponential fittings of their PL decay curves shown in Figure 4d. Moreover, the S peak from a single QD is linearly polarized while the B spectrum from the bulk material is completely unpolarized, as can be seen from the spectral evolution image plotted in Figure 4e as a function of the linear polarizer angle. This linear polarization of the S peak suggests that it should arise from one of the three bright-exciton states in a single perovskite QD,[56,57] which can efficiently accommodate the photoexcited charge carriers due to its lowest energy possibly caused by the shape anisotropy.[58] The above observations further confirm that the B spectrum should originate from the bulk material instead of the phonon side band of the S peak, in which case they would demonstrate very similar PL decay, linear polarization and single-photon emission features. Moreover, the B spectrum could be located on the red (Figure 4a) or blue (Figure 3e) side of the S peak, and their respective energy positions and mutual energy separations are plotted in the statistical histograms of Figure S7 in the Supporting Information.

Interestingly, the other sharp PL peaks resolved in Figure 4e with smaller intensities have their linear polarizations parallel to that of the S peak, implying that their corresponding QDs are formed in the single $CsPbBr_3$ microcrystal with the same direction of the elongated confinement potentials. To gain further insight into this confinement potential, we perform temperature-dependent optical measurements on the S peak of the same single $CsPbBr_3$ microcrystal. As can be seen in Figure 4f with the increasing temperature, the S peak is shifted to the blue side with a decreasing intensity until it is completely quenched at ≈28 K. PL intensity of the S peak can be recovered to the initial value when the sample temperature is returned back to ≈4 K, thus highlighting the shallow nature of the confinement potential. In Figure S8 in the Supporting Information, we present similar temperature-dependent optical properties measured for another single $CsPbBr_3$ microcrystal in the islanded film, whose main sharp PL peak is quenched at ≈36 K with a slightly deeper confinement potential than that discussed in Figure 4f.

3. Conclusion

To summarize, we have fabricated three types of all-inorganic perovskite films with different densities of single $CsPbBr_3$ microcrystals, and revealed at 4 K that single-photon emitters are universally present as a result of the local thickness variation. PL intensities of such single-photon emitters are completely quenched above ≈30 K due to their shallow confinement potentials, thus firmly distinguishing them from the blinking objects commonly observed at the room temperature due to the activation and passivation of super traps.[33] Beyond these blinking objects and the well-known inhomogeneous distribution of microscale emission regions, the novel observation of nanoscale quantum emitters in a perovskite film has greatly extended the current understanding of its intrinsic structure–property relationships. PL linewidths of these quantum emitters are close to those from several hundreds of μeV to ≈1 meV previously measured for the single $CsPbBr_3$ QDs,[57,59] although their single-photon emission purities are partially degraded by the background fluorescence from the bulk material. This problem could be solved in future works by a judicious growth of deeper confinement potentials, so that the photoexcited charge carriers in a single microcrystal can be dominantly localized into the single-photon emitters. As a reward of this additional effort, it is feasible to obtain electrically pumped single-photon sources based on single $CsPbBr_3$ microcrystals, by taking advantage of the mature techniques routinely applied to bulk perovskite materials for the fabrication of light-emitting diodes.[60]

4. Experimental Section

Materials: Lead bromide ($PbBr_2$, ≥99.99%) and caesium bromide (CsBr, ≥99.99%) were purchased from Xi'an Polymer Light Technology, anhydrous *N*,*N*-dimethylformamide (DMF, ≥99.8%), and dimethyl sulfoxide (DMSO, ≥99.9%) were purchased from Sigma-Aldrich, while isopropanol (IPA, ≥98.5%) and 2-methoxyethanol (EGME, ≥99.0%) were purchased from Sinopharm Chemical Reagent.

Fabrication: The compact $CsPbBr_3$ film was fabricated by a two-step solution method in the ambient air. 50 µL of the 75 °C DMF solution containing 1.0 mol L^{-1} $PbBr_2$ was spin-coated onto a glass substrate at the speed of 2000 rpm for 30 s. After being annealed at 75 °C for 30 min on a hot plate, the $PbBr_2$ precursor film was immersed faceup for 40 min in an EGME/IPA solution containing 15 mg mL^{-1} CsBr at the room temperature. The resulting sample was rinsed with IPA, dried in air and annealed at 250 °C for 5 min on a hot plate to obtain the compact $CsPbBr_3$ film. The porous $CsPbBr_3$ film was fabricated according to a similar procedure to that described above, except that the CsBr EGME/IPA solution was replaced by the CsBr EGME solution, and the $PbBr_2$ precursor film was immersed in the CsBr EGME solution for 10 min.

The islanded $CsPbBr_3$ film was fabricated by the single-step deposition method. The 0.1 M $CsPbBr_3$ precursor was prepared by dissolving the stoichiometric-ratio $PbBr_2$ and CsBr into a DMSO solution. The $CsPbBr_3$ precursor solution was then diluted by 30 times and the amount of 40 µL was spin-coated onto a glass substrate at the speed of 3000 rpm for 30 s. Finally, the sample was annealed at 160 °C for 10 min on a hot plate, so that the $CsPbBr_3$ film was formed with well-isolated single

microcrystals on top of a substrate. For convenience, this sample was denoted as "islanded film" to be consistent with the "compact film" and "porous film" used for the other two samples, although the single $CsPbBr_3$ microcrystals here are not surrounded by any continuous film.

Characterization: For the room-temperature optical measurements, the sample substrate was positioned in a home-built confocal scanning optical microscope and excited at 405 nm by a picosecond pulsed laser operated at the repetition rate of 5.6 MHz. The laser beam was focused to a spot diameter of ≈300 nm by an immersion-oil objective with a numerical aperture of 1.4, which was also used to collect the optical signal emitted from the $CsPbBr_3$ film. After passing through a 0.5 m spectrometer, the optical signal was sent to a charge-couple-device camera for the PL spectral measurement with an integration time of 1 s. Alternatively, the optical signal could pass through a 50/50 beam splitter and arrive at two avalanche photodiodes for the spatial image construction, as well as for the PL decay and second-order photon correlation measurements with a time resolution of ≈100 ps. For the latter two optical measurements, a spectral resolution of ≈1 meV is used to select either the sharp PL peak or the background spectrum emitted from a single $CsPbBr_3$ microcrystal, by narrowing down the exit slit of the spectrometer before the photons can arrive at the avalanche photodiodes.

For the cryogenic-temperature optical characterizations, the sample substrate was attached to the cold finger of a helium-free cryostat and excited at 520 nm by a picosecond pulsed laser operated at the repetition rate of 5.59 MHz. The laser beam was focused to a spot diameter of ≈3 μm by a dry objective with a numerical aperture of 0.8, which was also used to collect the optical signal emitted from the $CsPbBr_3$ film. The other experimental configurations are similar to those described above for the room-temperature measurement, except that a half wave plate and a linear polarizer are inserted into the signal collection path for characterizing the polarization-dependent optical properties. In this case, the excitation laser beam at 520 nm is circularly polarized while the half wave plate is attached to a motor-driven stage and rotated with a precision of 1°.

Supporting Information

Supporting Information is available from the Wiley Online Library or from the author.

Acknowledgements

Conflict of Interest

The authors declare no conflict of interest.

Data Availability Statement

The data that support the findings of this study are available from the corresponding author upon reasonable request.

Keywords

[1] A. Kojima, K. Teshima, Y. Shirai, T. Miyasaka, *J. Am. Chem. Soc.* **2009**, *131*, 6050.

[2] K. Lin, J. Xing, L. Quan, F. P. G. de Arquer, X. Gong, J. Lu, L. Xie, W. Zhao, D. Zhang, C. Yan, W. Li, X. Liu, Y. Lu, J. Kirman, E. H. Sargent, Q. Xiong, Z. Wei, *Nature* **2018**, *562*, 245.

[3] Z. Li, J. Moon, A. Gharajeh, R. Haroldson, R. Hawkins, W. Hu, A. Zakhidov, Q. Gu, *ACS Nano* **2018**, *12*, 10968.

[4] J. Feng, C. Gong, H. Gao, W. Wen, Y. Gong, X. Jiang, B. Zhang, Y. Wu, Y. Wu, H. Fu, L. Jiang, X. Zhang, *Nat. Electron.* **2018**, *1*, 404.

[5] Y. Lei, Y. Chen, R. Zhang, Y. Li, Q. Yan, S. Lee, Y. Yu, H. Tsai, W. Choi, K. Wang, Y. Luo, Y. Gu, X. Zheng, C. Wang, C. Wang, H. Hu, Y. Li, B. Qi, M. Lin, Z. Zhang, S. A. Dayeh, M. Pharr, D. P. Fenning, Y.-H. Lo, L. Jian, K. Yang, J. Yoo, W. Nie, S. Xu, *Nature* **2020**, *583*, 790.

[6] H.-S. Kim, C.-R. Lee, J.-H. Im, K.-B. Lee, T. Moehl, A. Marchioro, S.-J. Moon, R. Humphry-Baker, J.-H. Yum, J. E. Moser, M. Grätzel, N.-G. Park, *Sci. Rep.* **2012**, *2*, 591.

[7] J. Burschka, N. Pellet, S.-J. Moon, R. Humphry-Baker, P. Gao, M. K. Nazeeruddin, M. Grätzel, *Nature* **2013**, *499*, 316.

[8] W. S. Yang, J. H. Noh, N. J. Jeon, Y. C. Kim, S. Ryu, J. Seo, S. I. Seok, *Science* **2015**, *348*, 1234.

[9] J. J. Yoo, G. Seo, M. R. Chua, T. G. Park, Y. Lu, F. Rotermund, Y.-K. Kim, C. S. Moon, N. J. Jeon, J.-P. Correa-Baena, V. Bulović, S. S. Shin, M. G. Bawendi, J. Seo, *Nature* **2021**, *590*, 587.

[10] National Renewable Energy Laboratory. Best Research-Cell Efficiency Chart, https://www.nrel.gov/pv/cell-efficiency.html (accessed: August 2021).

[11] J.-P. Correa-Baena, M. Saliba, T. Buonassisi, M. Grätzel, A. Abate, W. Tress, A. Hagfeldt, *Science* **2017**, *358*, 739.

[12] J.-W. Lee, D.-H. Kim, H.-S. Kim, S.-W. Seo, S. M. Cho, N.-G. Park, *Adv. Energy Mater.* **2015**, *5*, 1501310.

[13] B. Conings, J. Drikoningen, N. Gauquelin, A. Babayigit, J. D'Haen, L. D'Olieslaeger, A. Ethirajan, J. Verbeeck, J. Manca, E. Mosconi, F. D. Angelis, H.-G. Boyen, *Adv. Energy Mater.* **2015**, *5*, 1500477.

[14] C. M. Sutter-Fella, Q. P. Ngo, N. Cefarin, K. L. Gardner, N. Tamura, C. V. Stan, W. S. Drisdell, A. Javey, F. M. Toma, I. D. Sharp, *Nano Lett.* **2018**, *18*, 3473.

[15] J. Liang, C. Wang, Y. Wang, Z. Xu, Z. Lu, Y. Ma, H. Zhu, Y. Hu, C. Xiao, X. Yi, G. Zhu, H. Lv, L. Ma, T. Chen, Z. Tie, Z. Jin, J. Liu, *J. Am. Chem. Soc.* **2016**, *138*, 15829.

[16] M. Kulbak, D. Cahen, G. Hodes, *J. Phys. Chem. Lett.* **2015**, *6*, 2452.

[17] R. E. Beal, D. J. Slotcavage, T. Leijtens, A. R. Bowring, R. A. Belisle, W. H. Nguyen, G. F. Burkhard, E. T. Hoke, M. D. McGehee, *J. Phys. Chem. Lett.* **2016**, *7*, 746.

[18] R. J. Sutton, G. E. Eperon, L. Miranda, E. S. Parrott, B. A. Kamino, J. B. Patel, M. T. Hörantner, M. B. Johnston, A. A. Haghighirad, D. T. Moore, H. J. Snaith, *Adv. Energy Mater.* **2016**, *6*, 1502458.

[19] Z. Li, L. Kong, S. Huang, L. Li, *Angew. Chem., Int. Ed.* **2017**, *56*, 8134.

[20] X. Han, X. Wang, J. Feng, H. Huang, Z. Zhu, T. Yu, Z. Li, Z. Zou, *ACS Appl. Electron. Mater.* **2021**, *3*, 373.

[21] J. Li, J. Feng, H. Huang, Z. Zhu, X. Han, T. Yu, Z. Li, Z. Zou, *Appl. Phys. Lett.* **2021**, *118*, 221604.

[22] J. Duan, Y. Zhao, B. He, Q. Tang, *Angew. Chem., Int. Ed.* **2018**, *57*, 3787.

[23] X. Li, Y. Tan, H. Lai, S. Li, Y. Chen, S. Li, P. Xu, J. Yang, *ACS Appl. Mater. Interfaces* **2019**, *11*, 29746.

[24] Y. Zhao, J. Duan, H. Yuan, Y. Wang, X. Yang, B. He, Q. Tang, *Sol. RRL* **2019**, *3*, 1800284.

**ADVANCED
SCIENCE NEWS**
www.advancedsciencenews.com

**ADVANCED
MATERIALS**
www.advmat.de

[25] X. Liu, X. Tan, Z. Liu, H. Ye, B. Sun, T. Shi, Z. Tang, G. Liao, *Nano Energy* **2019**, *56*, 184.

[26] G. Tong, T. Chen, H. Li, L. Qiu, Z. Liu, Y. Dang, W. Song, L. K. Ono, Y. Jiang, Y. Qi, *Nano Energy* **2019**, *65*, 104015.

[27] J. Duan, Y. Zhao, Y. Wang, X. Yang, Q. Tang, *Angew. Chem., Int. Ed.* **2019**, *58*, 16147.

[28] D. W. de Quilettes, S. M. Vorpahl, S. D. Stranks, H. Nagaoka, G. E. Eperon, M. E. Ziffer, H. J. Snaith, D. S. Ginger, *Science* **2015**, *348*, 683.

[29] T. A. S. Doherty, A. J. Winchester, S. Macpherson, D. N. Johnstone, V. Pareek, E. M. Tennyson, S. Kosar, F. U. Kosasih, M. Anaya, M. Abdi-Jalebi, Z. Andaji-Garmaroudi, E. L. Wong, J. Madéo, Y.-H. Chiang, J.-S. Park, Y.-K. Jung, C. E. Petoukhoff, G. Divitini, M. K. L. Man, C. Ducati, A. Walsh, P. A. Midgley, K. M. Dani, S. D. Stranks, *Nature* **2020**, *580*, 360.

[30] Y. Tian, A. Merdasa, E. Unger, M. Abdellah, K. Zheng, S. McKibbin, A. Mikkelsen, T. Pullerits, A. Yartsev, V. Sundström, I. G. Scheblykin, *J. Phys. Chem. Lett.* **2015**, *6*, 4171.

[31] E. T. Hoke, D. J. Slotcavage, E. R. Dohner, A. R. Bowring, H. I. Karunadasa, M. D. McGehee, *Chem. Sci.* **2015**, *6*, 613.

[32] W. Li, M. U. Rothmann, A. Liu, Z. Wang, Y. Zhang, A. R. Pascoe, J. Lu, L. Jiang, Y. Chen, F. Huang, Y. Peng, Q. Bao, J. Etheridge, U. Bach, *Adv. Energy Mater.* **2017**, *7*, 1700946.

[33] I. Y. Eremchev, A. O. Tarasevich, J. Li, A. V. Naumov, I. G. Scheblykin, *Adv. Opt. Mater.* **2021**, *9*, 2001596.

[34] A. J. Barker, A. Sadhanala, F. Deschler, M. Gandini, S. P. Senanayak, P. M. Pearce, E. Mosconi, A. J. Pearson, Y. Wu, A. R. S. Kandada, T. Leijtens, F. D. Angelis, S. E. Dutton, A. Petrozza, R. H. Friend, *ACS Energy Lett.* **2017**, *2*, 1416.

[35] X. Wen, A. Ho-Baillie, S. Huang, R. Sheng, S. Chen, H.-C. Ko, M. A. Green, *Nano Lett.* **2015**, *15*, 4644.

[36] M. Gerhard, B. Louis, R. Camacho, A. Merdasa, J. Li, A. Kiligaridis, A. Dobrovolsky, J. Hofkens, I. G. Scheblykin, *Nat. Commun.* **2019**, *10*, 1698.

[37] A. Merdasa, Y. Tian, R. Camacho, A. Dobrovolsky, E. Debroye, E. L. Unger, J. Hofkens, V. Sundström, I. G. Scheblykin, *ACS Nano* **2017**, *11*, 5391.

[38] D. K. Sharma, S. Hirata, M. Vacha, *Nat. Commun.* **2019**, *10*, 4499.

[39] J. Vogelsang, R. Kasper, C. Steinhauer, B. Person, M. Heilemann, M. Sauer, P. Tinnefeld, *Angew. Chem., Int. Ed.* **2008**, *47*, 5465.

[40] B. Lounis, W. E. Moerner, *Nature* **2000**, *407*, 491.

[41] M. Nirmal, B. O. Dabbousi, M. G. Bawendi, J. J. Macklin, J. K. Trautman, T. D. Harris, L. E. Brus, *Nature* **1996**, *383*, 802.

[42] P. Michler, A. Imamoğlu, M. D. Mason, P. J. Carson, G. F. Strouse, S. K. Buratto, *Nature* **2000**, *406*, 968.

[43] P. Frantsuzov, M. Kuno, B. Jankó, R. A. Marcus, *Nat. Phys.* **2018**, *4*, 519.

[44] B. Lounis, M. Orrit, *Rep. Prog. Phys.* **2005**, *68*, 1129.

[45] N. A. Lozing, M. G. Gladush, I. Y. Eremchev, E. A. Ekimov, A. V. Naumov, *Phys. Rev. B* **2020**, *102*, 060301.

[46] D. A. Vanden Bout, W.-T. Yip, D. Hu, D.-K. Fu, T. M. Swager, P. F. Barbara, *Science* **1997**, *277*, 1074.

[47] J. M. Lupton, *Adv. Mater.* **2010**, *22*, 1689.

[48] A. Francisco-López, B. Charles, O. J. Weber, M. I. Alonso, M. Garriga, M. Campoy-Quiles, M. T. Weller, A. R. Goñi, *J. Phys. Chem. Lett.* **2019**, *10*, 2971.

[49] R. Saran, A. Heuer-Jungemann, A. G. Kanaras, R. J. Curry, *Adv. Opt. Mater.* **2017**, *5*, 1700231.

[50] B. Lv, H. Zhang, L. Wang, C. Zhang, X. Wang, J. Zhang, M. Xiao, *Nat. Commun.* **2018**, *9*, 1536.

[51] Y.-M. He, Y. He, Y.-J. Wei, D. Wu, M. Atatüre, C. Schneider, S. Höfling, M. Kamp, C.-Y. Lu, J.-W. Pan, *Nat. Nanotechnol.* **2013**, *8*, 213.

[52] L. Protesescu, S. Yakunin, M. I. Bodnarchuk, F. Krieg, R. Caputo, C. H. Hendon, R. X. Yang, A. Walsh, M. V. Kovalenko, *Nano Lett.* **2015**, *15*, 3692.

[53] D. G. Suárez-Forero, M. Giuri, M. De Giorgi, L. Polimeno, L. De Marco, F. Todisco, G. Gigli, L. Dominici, D. Ballarini, V. Ardizzone, B. D. Belviso, D. Altamura, C. Giannini, R. Brescia, S. Colella, A. Listorti, C. E. Corcione, A. Rizzo, D. Sanvitto, *ACS Nano* **2019**, *13*, 10711.

[54] D. Gammon, E. S. Snow, B. V. Shanabrook, D. S. Katzer, D. Park, *Science* **1996**, *273*, 87.

[55] M. Gerhard, B. Louis, P. A. Frantsuzov, J. Li, A. Kiligaridis, J. Hofkens, I. G. Scheblykin, *Adv. Opt. Mater.* **2021**, *9*, 2001380.

[56] C. Yin, L. Chen, N. Song, Y. Lv, F. Hu, C. Sun, W. W. Yu, C. Zhang, X. Wang, Y. Zhang, M. Xiao, *Phys. Rev. Lett.* **2017**, *119*, 026401.

[57] M. Fu, P. Tamarat, H. Huang, J. Even, A. L. Rogach, B. Lounis, *Nano Lett.* **2017**, *17*, 2895.

[58] J. Liu, F. Hu, Y. Zhou, C. Zhang, X. Wang, M. Xiao, *J. Lumin.* **2020**, *221*, 117032.

[59] F. Hu, H. Zhang, C. Sun, C. Yin, B. Lv, C. Zhang, W. W. Yu, X. Wang, Y. Zhang, M. Xiao, *ACS Nano* **2015**, *9*, 12410.

[60] X.-K. Liu, W. Xu, S. Bai, Y. Jin, J. Wang, R. H. Friend, F. Gao, *Nat. Mater.* **2021**, *20*, 10.